Angular dependence of metamagnetic transitions in HoNi$_2$B$_2$C

P. C. Canfield, S. L. Bud'ko,[*] and B. K. Cho[†]

Ames Laboratory and Department of Physics and Astronomy, Iowa State University, Ames, Iowa 50011

A. Lacerda

National High Magnetic Field Laboratory–Pulse Facility, Los Alamos National Laboratory, Los Alamos, New Mexico 87545

D. Farrell and E. Johnston-Halperin

Department of Physics, Case Western Reserve University, Cleveland, Ohio 44106

V. A. Kalatsky and V. L. Pokrovsky

Department of Physics, Texas A&M University, College Station, Texas 77843

(Received 30 July 1996)

Detailed measurements of $M(2\text{ K}, H, \theta)$ of HoNi$_2$B$_2$C, where θ is the angle that the applied field H makes with the [110] axis while remaining perpendicular to the crystallographic c axis, reveal three metamagnetic transitions with angular dependences $H_{c1}=(4.1\pm0.1\text{ kG})/\cos(\theta)$, $H_{c2}=8.4\pm0.2\text{ kG}/\cos(\phi)$, and $H_{c3}=(6.6\pm0.2\text{ kG})/\sin(\phi)$, where $\phi=\theta-45$ is the angle from the [100] axis. The high-field saturated moment, $M_{\text{sat}}\approx10\mu_B\cos\theta$ is consistent with the local moments being confined to the [110] direction. The locally saturated moments for fields between H_{ci} ($i=1,2,3$) also manifest angular dependences that are consistent with combinations of local moments along [110] axes. Analysis of these data lead us to infer that the net distribution of moments is $(\uparrow\downarrow\uparrow\downarrow\uparrow\downarrow)$ for $H<H_{c1}$, $(\uparrow\uparrow\downarrow\uparrow\uparrow\downarrow)$ for $H_{c1}<H<H_{c2}$, $(\uparrow\uparrow\rightarrow\uparrow\uparrow\rightarrow)$ for $H_{c2}<H<H_{c3}$, and $(\uparrow\uparrow\uparrow\uparrow\uparrow\uparrow)$ for $H>H_{c3}$. [S0163-1829(97)02902-0]

INTRODUCTION

The RNi$_2$B$_2$C (R=Gd–Lu, and Y) series continues to yield new features of interest. For R=Y and Lu the superconducting transition temperatures T_c are approximately 15 and 16 K, respectively,[1,2] while for R=Tm, Er, and Ho superconductivity and antiferromagnetic order coexist for $T<T_N<T_c$,[3–8] where T_N is the antiferromagnetic ordering temperature. In DyNi$_2$B$_2$C the progression of the ordering temperatures is reversed, giving rise to a rare example of a compound, with nonhybridizing $4f$ electrons, with $T_c<T_N$.[9] Recently single crystals of YbNi$_2$B$_2$C have been grown,[10] and while it is not a superconductor for $T>0.35$ K, it is a heavy fermion compound with a Sommerfeld coefficient of $\gamma=530$ mJ/mol K^2. TbNi$_2$B$_2$C and GdNi$_2$B$_2$C do not manifest superconductivity for $T>2$ K,[11,12] but TbNi$_2$B$_2$C has a phase transition from antiferromagnetic order ($T<15$ K) to an ordered state that has a weak ferromagnetic component of 0.5 μ_B/Tb for $T<8$ K.[11]

The RNi$_2$B$_2$C materials have extremely anisotropic magnetic properties for R=Er,[6,13] Ho,[7,8,14,15] Dy,[9] and Tb.[11,16] Due to crystalline electric field (CEF) splitting of the ground-state multiplet of the R^{+3} ion, the moments for R=Er–Tb are essentially confined to the basal a-b plane for temperatures comparable to and below T_N and T_c.[6–9,11,13–16] (The lower-energy CEF splittings and levels have been determined in detail[15] for R=Ho.) This anisotropy manifests itself in the temperature dependent magnetization $M(T)$, as well as in the field-dependent magnetization $M(H)$ isotherms. The effects of these anisotropies also appear in upper superconducting critical field $H_{c2}(T)$ and $T_N(H)$ phase diagrams.[4,6,8,17] In addition to the anisotropy found between magnetization data collected with the field applied parallel and perpendicular to the crystallographic c axis, there is a substantial anisotropy between the magnetization for the field applied along the [100] and [110] axes, both of which are perpendicular to the [001] (c axis).

For HoNi$_2$B$_2$C, this anisotropy between the magnetization with the field applied along the [100] axis, M_{100}, and the magnetization with the field applied along the [110] axis, M_{110}, manifests itself not only in the high-field saturated magnetization,[15] but also in the critical field values of the two metamagnetic phase transitions found at $T=2$ K for $H<50$ kG for these two orientations.[7,8,17] Finally, for the applied field perpendicular to the c axis, but not along one of the two principle in-plane axes, there can be three metamagnetic phase transitions at $T=2$ K for $H<50$ kG.[7] These data indicate that there may be a rich angular dependence of the $M(T=2\text{ K}, H)$.

In this paper we present a study of the angular dependence of $M(T=2\text{ K}, H, \theta)$ for HoNi$_2$B$_2$C. As a result of this study, we show that remarkably simple geometric relationships exist between the critical fields of the three metamagnetic phase transitions and the angle the applied field makes with respect to the nearest [110] axis. Similar simple angular dependences emerge for the high-field-saturated moment as well as the locally saturated magnetization plateaus found for fields between the metamagnetic transitions.

After an overview of the experimental techniques used to grow and characterize these crystals, we will present our data and discuss how our results lead to a simple picture of the net distribution of moments along the [110] axes.

EXPERIMENTAL METHODS

Single crystals of $HoNi_2B_2C$ were grown using the Ames Lab Ni_2B flux-growth technique.[2,6] Polycrystalline samples of $HoNi_2B_2C$ were synthesized by arc-melting together stoichiometric amounts of Ho (99.99 Ames Lab), Ni (99.9), B (99 atomic and 99.5 B-11 isotopic, Eagle Picher), and C (99.99). The polycrystalline $HoNi_2B_2C$ was then heated with an equal weight of Ni_2B in a Al_2O_3 crucible under a flowing Ar atmosphere to 1490 °C and cooled to 1200 °C over 60 h. The growth was then cooled to room temperature and the single-crystal samples were removed from the remaining Ni_2B flux.

This technique can yield single crystals as large as 800 mg that have the form of plates as large as $10 \times 7 \times 0.75$ mm^3. The crystallographic c axis of the tetragonal unit cell[18] is perpendicular to the surface of the plate. In addition the crystals tend to facet along the [100] axis.

The majority of the magnetization measurements have been carried out in a Quantum Design (QD), superconducting quantum interference device (SQUID) magnetometer. A modified version of the QD sample rotator probe, that allows for the rotation of the sample in a manner that keeps the c axis approximately perpendicular to the applied field at all times, was used. Due to the large sample moment and the large anisotropies associated with the sample magnetization, a small sample mass of approximately 0.5 mg was used with the rotator probe. This was necessary so as to avoid torques large enough to cause slippage of the rotor. In order to eliminate uncertainty associated with weighing errors, M_{100}, M_{110}, and M_{001} were measured on samples weighing up to two orders of magnitude more. The magnetization data from the rotator was normalized to the M_{110} data, leading to perfect agreement with the M_{100} data. The rotator has a relative angular uncertainty of less than 1°, but due to the small sample size and the nature of the probe, there is an uncertainty associated with the angle that the c axis makes with the applied field. Instead of being exactly perpendicular, there is the possibility that the c axis makes a cone of revolution about the desired normal to the applied field. The angle of this cone of rotation is anticipated to be small, but it is poorly determined in the experimental set up. This angle is estimated to be less than 10°.

High magnetic-field magnetization data were collected for fields up to 180 kG using a vibrating-sample magnetometer (VSM) located at the National High Magnetic Field Laboratory-Pulsed Facility in Los Alamos. A platelike sample weighing 28 mg was attached to a plastic disk that was rigidly oriented with respect to the applied field at the onset of each run. Given the larger sample surface area, we were able to more accurately determine that $H \perp c$, but since the angle that the applied field made with respect to the [100] axis was determined by eye, the error bars associated with the orientation of the field in the a-b plane are large and are estimated to be ±4°.

On the other extreme, precise determinations of the first, low-field, metamagnetic phase transition, H_{c1}, were made using torque magnetometery techniques. A piece of crystal weighing approximately 0.05 mg was cleaved from a larger sample and mounted so the the applied field could be rotated in the a-b plane. Data were collected at 4.28 K and H_{c1} was
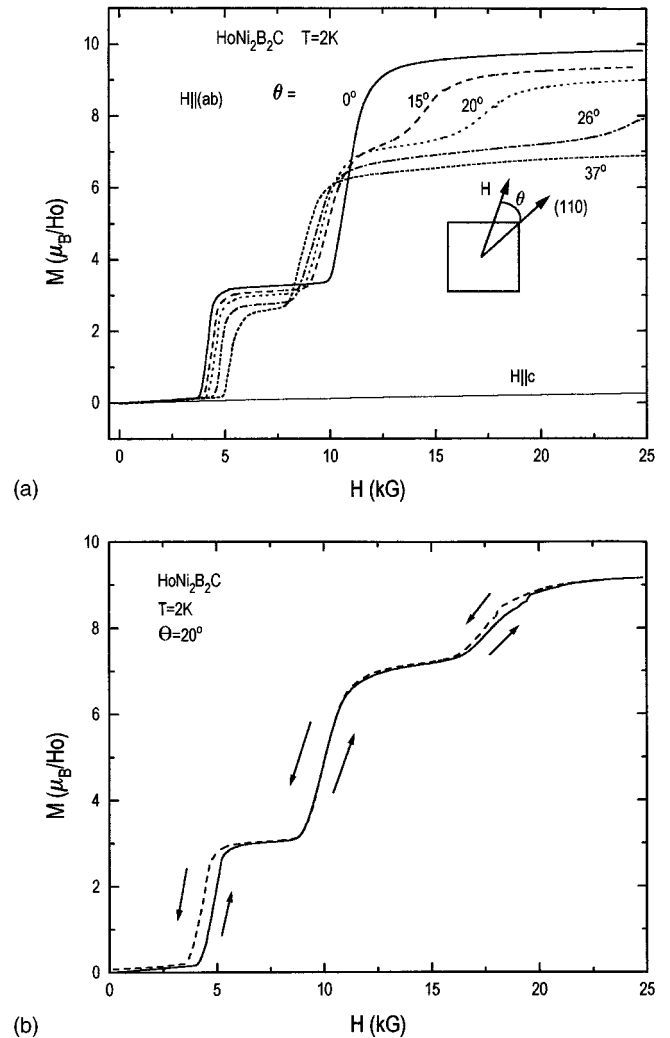

FIG. 1. (a) Magnetization M versus applied field of H of $HoNi_2B_2C$ at $T=2$ K for $H \| c$ and $H \perp c$. For $H \perp c$, the applied field makes an angle θ with respect to the [110] crystallographic axis (see inset). (b) M versus H for $\theta=20°$ for increasing and decreasing field.

determined to within 50 G by observing an extremely sharp torque transition at the H_{c1} phase boundary. This is the only data set not taken at 2 K and the effects of elevated temperature will be discussed below.

DATA

$M(2$ K, H, $\theta)$ data are shown in Fig. 1(a) for representative angles of applied magnetic field. With the exception of the $H \| c$ data, H is approximately perpendicular to the c axis. θ is the angle the applied field in the tetragonal plane makes with respect to the nearest [110] axis. M_{110} $(\theta=0°)$ is the easy magnetic axis and at high fields M_{110} approaches $10\mu_B$. There are clear metamagnetic transitions in the M_{110} data at $H_{c1}=4.1$ kG and $H_{c2}=10.7$ kG. For fields below H_{c1} the structure of the magnetically ordered moments is simple antiferromagnetic.[14] Whole a-b planes of Ho moments align ferromagnetically, and these sheets are rotated by 180° with respect to each other along the c axis. As the angle θ between the applied field and the [110] axis increases, H_{c1}
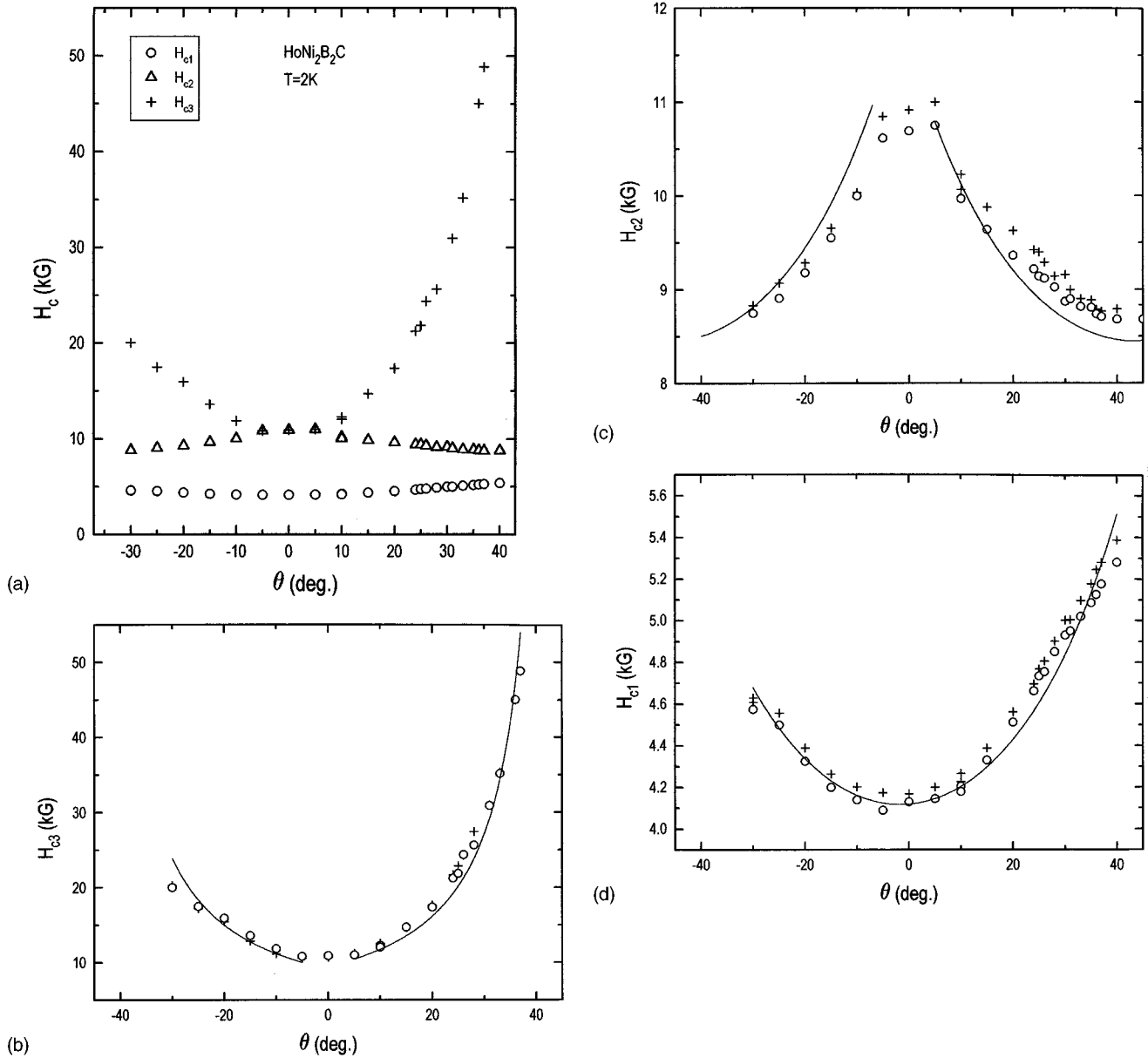
FIG. 2. (a) Critical magnetic fields H_{c1} (circles), H_{c2} (triangles), and H_{c3} (crosses) of $HoNi_2B_2C$ versus angle in tetragonal basal plane from [110], θ. (b) H_{c3} versus θ, solid line is $H_{c3} = 6.6$ kG/sinϕ, where $\phi = 45 - \theta$. (c) H_{c2} versus θ, solid line is $H_{c2} = 8.4$ kG/cos ϕ. (d) H_{c1} versus θ, solid line is $H_{c1} = 4.1$ kG/cos θ. Note: For (b)–(d) determination of H_{ci} via both maximum dM/dH (circles) and midpoint of transition (crosses) are shown.

increases, H_{c2} decreases, and a third metamagnetic phase transition, H_{c3}, separates itself from H_{c2} and increases rapidly. In addition, as θ increases, the size of the jump (ΔM_3) in the magnetization at H_{c3} as well as high-field saturated moment (M_{sat}), decrease.

All of the data in Fig. 1(a) has been collected for increasing applied magnetic field. Figure 1(b) presents data collected on increasing and decreasing applied field for $\theta = 20°$. H_{c1} and H_{c3} manifest modest hysterisis and H_{c2} is not hysteretic to within our resolution. The size of the hysterisis changes only slightly with θ. For the rest of this paper only data taken for increasing field will be considered.

Metamagnetic transitions are clearly seen in Fig. 1. The value of the critical fields of the phase transitions can be determined by using the local maxima in dM/dH. Using this criterion, Fig. 2(a) shows the angular dependence of H_{c1},

H_{c2}, and H_{c3}. Figures 2(b)–2(d) display enlargements of these data with the critical field determined from both the maximum dM/dH as well as the midpoint of the transition. As can be seen there is very little difference between the two criteria. The data shown in Fig. 2 are consistent with a four-fold symmetry associated with the tetragonal basal plane. For $\theta > 45°$, H_{c1} and H_{c3} decrease, while H_{c2}, having passed through a local minimum at $\theta = 45$, starts to increase again.

In order to examine the angular dependence of H_{c1} in greater detail magnetotorque measurements were performed at $T = 4.28$ K. As the applied field is increased from $H < H_{c1}$ to $H > H_{c1}$ there is a sudden increase in the torque on the sample. The field at which the sudden onset of torque on the sample is observed is plotted in Fig. 3 as a function of θ. There is a clear periodicity to the data, with a local minima for $H\|[110]$ and a sharp local maxima for $H\|[100]$. Unfortu-
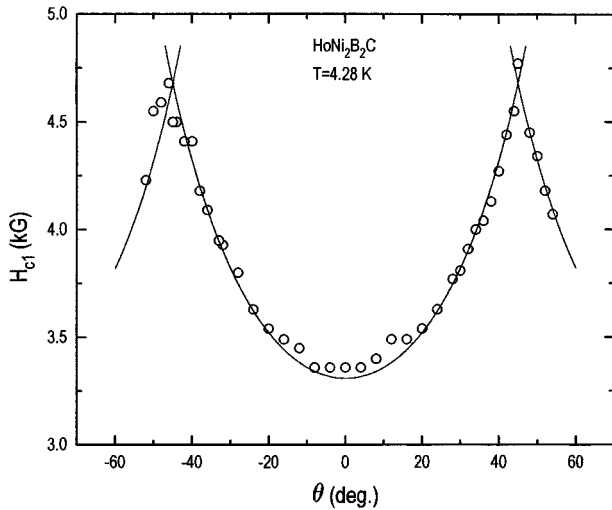
FIG. 3. H_{c1} versus θ of HoNi$_2$B$_2$C for $T=4.28$ K as determined via magnetotorque measurements. Solid line $H_{c1}=3.3$ kG/cosθ.

nately, due to the large forces on the sample for $H>H_{c1}$, the magnetotorque apparatus used for these measurements was not able to resolve subsequent metamagnetic transitions.

H_{c3} rapidly increases as $\theta\rightarrow45°$. In order to determine to how high a field H_{c3} continues to exist, we measured $M(2$ K, H, $\theta)$ for fields up to 180 kG. These data are shown in Fig. 4(a) and the $H_{c3}(\theta)$ diagram is show in Fig. 4(b). The transition can be clearly seen for fields up to 100 kG, and if finer angular resolution had been available it seems likely that for θ closer to 45° H_{c3} could approach 150 or 200 kG.

In addition to the angular dependence of the critical fields of the metamagnetic transitions there is an angular dependence to the saturated moment for various field ranges. For $H>H_{c3}$ the magnetization approaches a saturation value. Figure 5(a) presents saturated magnetization data from measurements taken using the QD sample rotator on both HoNi$_2$B$_2$C and (Ho$_{0.02}$Lu$_{0.98}$)Ni$_2$B$_2$C samples. The data were taken at 50 kG, rotating the sample in the applied field between data points. Both the dilute and concentrated Ho samples manifest a simple angular dependence of the saturated moment. For HoNi$_2$B$_2$C there is the possibility of H_{c3} moving through 50 kG as $\theta\rightarrow45°$, but as shown in Figs. 1(a) and 4(a), the jump in magnetization (ΔM_3) at H_{c3} decreases as H_{c3} increases, leading to no distinct feature in the pure HoNi$_2$B$_2$C data shown in Fig. 5(a). For both dilute and concentrated Ho, there is a broad, local maximum for the field applied along the [110] direction.

For values of the applied field $H_{c1}<H<H_{c2}$ there is a plateau in magnetization [Fig. 1(a)]. Since this plateau exists over a limited range of fields, it is hard to uniquely determine its saturation value so saturation values M_{sat1} based on (i) linear extrapolation of the plateau back to zero applied field (circles), and (ii) the midpoint value of magnetization $M([H_{c1}+H_{c2}]/2)$ (crosses), are plotted in Fig. 5(b). Both criteria yield data sets with a broad maximum for $H\|[110]$. Since H_{c2} and H_{c3} merge for θ close to 0°, the saturated moment for $H_{c2}<H<H_{c3}$, M_{sat2}, cannot be determined for all θ values. In addition, since H_{c3} increases rapidly as θ is increased, it is even more difficult to choose a unique criteria for determining $M_{sat2}(\theta)$. Data for M_{sat2} (2 K, 13 kG, θ) are
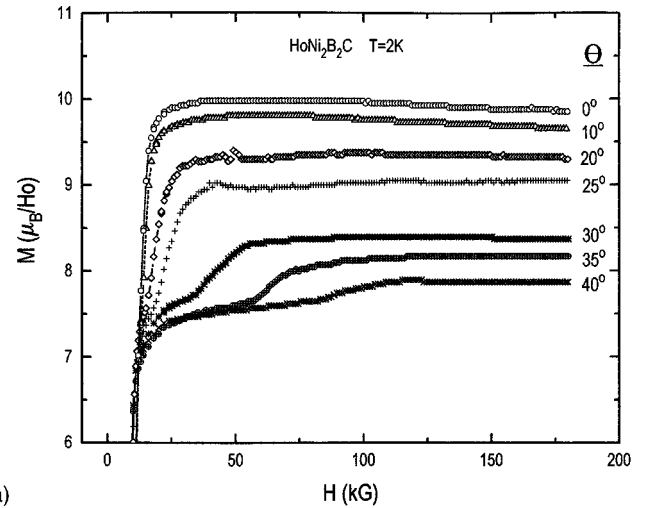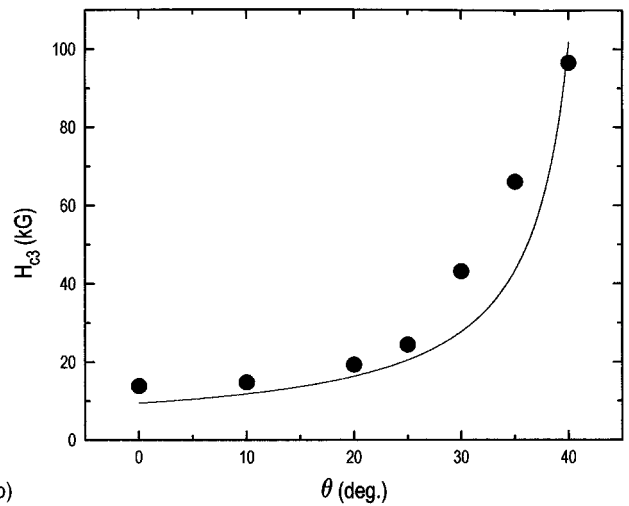
FIG. 4. (a) High-field M versus H HoNi$_2$B$_2$C for various angles θ. (b) H_{c3} versus θ as determined from data in (a). The solid line is $H_{c3}=6.6$ kG/sinϕ as determine from Fig. 2(b).

shown in Fig. 5(c) for θ values that manifest separated H_{c2} and H_{c3}.

One other parameter that can be easily measured as a function of θ is the jump in magnetization at H_{c3} (ΔM_3) which is plotted in Fig. 5(d) using both lower field and higher field data sets shown in Figs. 1(a) and 4(a). ΔM_3, was determined by linearly extrapolating the $H>H_{c3}$ $M(H)$ data to $H<H_{c3}$ and the $H<H_{c3}$ $M(H)$ data to $H>H_{c3}$ and measuring the difference in M between these two extrapolations at $H=H_{c3}$.

ANALYSIS

Figure 5(a) clearly demonstrates the CEF-induced anisotropy of the Ho^{3+} moments in HoNi$_2$B$_2$C at $T=2$ K. The $M(2$ K, 50 kG, $\theta)$ data for (Ho$_{0.02}$Lu$_{0.98}$)Ni$_2$B$_2$C are well fit by $(9.85\mu_B)\cos(\theta)$, shown as the solid line in the figure. The HoNi$_2$B$_2$C data follow a similar angular dependency, but deviate from the dilute (Ho$_{0.02}$Lu$_{0.98}$)Ni$_2$B$_2$C data slightly. This is probably due to interactions between the Ho sites (as manifest by H_{c3}). These angular dependences are consistent with the Ho moment being fully along the [110] direction.
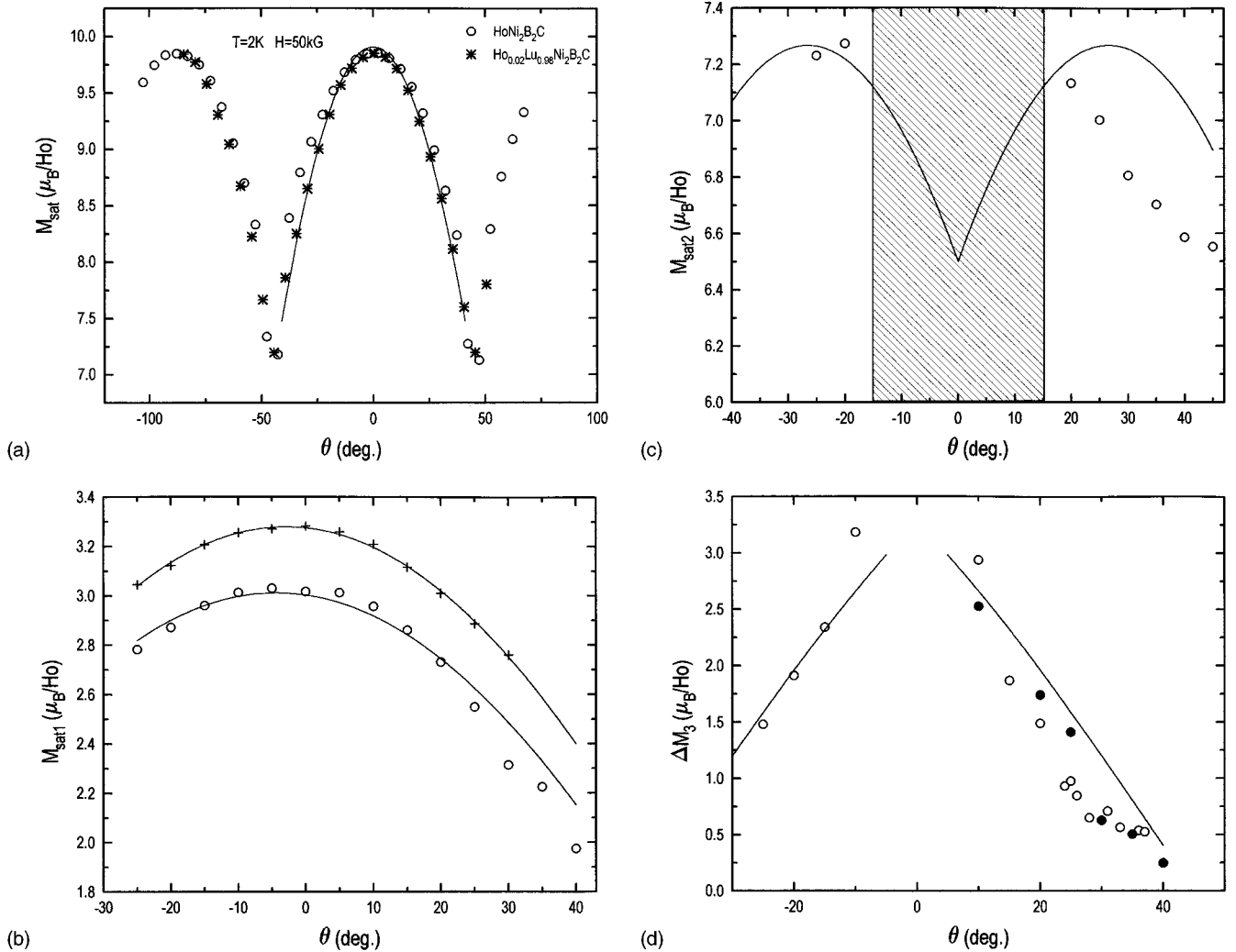
FIG. 5. (a) Magnetization of $HoNi_2B_2C$ and $(Lu_{0.98}Ho_{0.02})Ni_2B_2C$ versus θ for $T=2$ K and $H=50$ kG (M_{sat}) versus θ. Solid line is $M_{sat}=9.85\mu_B\cos\theta$. (b) Locally saturated magnetization for $H_{c1}<H<H_{c2}$ (M_{sat1}) versus θ determined by two different criteria, see text. Solid lines are $3.25\mu_B\cos\theta$ and $3.00\mu_B\cos\theta$. (c) Locally saturated magnetization for $H_{c2}<H=13$ kG$<H_{c3}$ (M_{sat2}) versus θ. Solid line is $3.25\mu_B$ ($2\cos\theta+\sin\theta$). Note that the grey zone is the region for which M_{sat2} is not measurable. (d) Jump in magnetization at H_{c3} (ΔM_3) versus θ. The open and filled symbols are from SQUID and VSM data sets, respectively. The solid line is $4.64\mu_B\sin\phi$.

This would lead to the longitudinal moment measured by the SQUID magnetometer varying as $\mu_{sat}\cos(\theta)$.

Figure 5(b) displays a similar angular dependence of the magnetization plateau M_{sat1} for fields between H_{c1} and H_{c2}. In this case the magnetization varies as $(3.25\mu_B)\cos(\theta)$ where it should be noted that $3.25\mu_B$ is very close to $\mu_{sat}/3$. Two features of this simple angular dependence merit attention. First, the fact that the magnetization varies as $\cos(\theta)$ again indicates that the net moment is along a [110] axis. Second, the prefactor being essentially $M_{sat}/3$ strongly suggests that this first metamagnetic state is simply related to moment arrangements such as ($\uparrow\uparrow\downarrow\uparrow\uparrow\downarrow$) where the moments are along [110] axes. This interpretation of the angular dependence of these data implies that the sample is a single magnetic domain for fields above H_{c1}, therefore it is likely that the metamagnetic transition at H_{c1} consists of both a change in magnetic structure and a spin flop of domains.

In addition to the angular dependences of the saturated moments, clear angular dependences of the critical magnetic fields H_{c1}, H_{c2}, and H_{c3} are apparent in Figs. 1–4. This is

most simply seen in the H_{c1} data. Figure 3 manifests a simple $H_{c1}^0/\cos\theta$ dependence where H_{c1}^0 is a multiplicative constant equal to the value of H_{c1} at $\theta=0°$. The solid line in Fig. 3 is a fit to this form with $H_{c1}^0=3.3$ kG. The H_{c1} data in Fig. 2(d) have a similar angular dependence, but in this case there is a slight asymmetry associated with the deviation of the direction of the applied field from the tetragonal a-b plane. The solid line in Fig. 2(d) is of the form $H_{c1}=H_{c1}^0/\cos(\theta)$ with $H_{c1}^0=4.1\pm0.1$ kG. The 20% decrease in H_{c1}^0 upon raising the temperature from 2.0 K [Fig. 2(d)] to 4.28 K (Fig. 3) is fully consistent with the temperature-field phase diagram for $HoNi_2B_2C$ for $H\parallel[100]$ presented by Rathnayaka *et al.*,[8] which shows a decrease of approximately 20%.

H_{c2} and H_{c3} have equally simple and suggestive angular dependences. While H_{c2} remains finite over the whole range of angles of the applied field [Fig. 2(c)], H_{c3} seems to diverge as $\theta\rightarrow45°$ [Figs. 2(b) and 4(b)]. This behavior is consistent with H_{c2} and H_{c3} also having simple angular dependences on inverse trigonometric functions. H_{c2} can be fit to
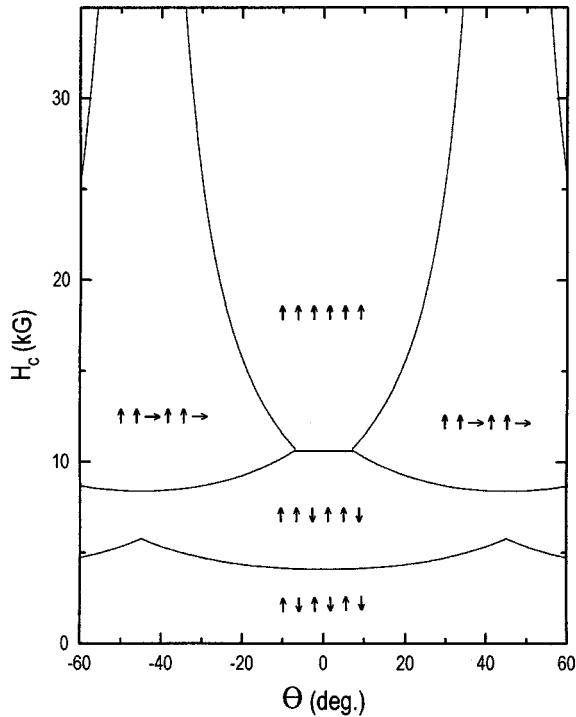
FIG. 6. Schematic H-θ phase diagram with net distribution of moments show for each of four regions. Note that moments are solely along [110] axes.

$H_{c2}=H^0_{c2}/\cos\phi$, where ϕ is the angle that the applied field makes with the nearest [100] axis ($\phi=45-\theta$) and $H^0_{c2}=8.4\pm0.2$ kG. By the same token, $H_{c3}=H^0_{c3}/\sin\phi$, where $H^0_{c3}=6.6\pm0.2$ kG, leading to H_{c3} diverging as $\phi\rightarrow90$. The solid lines in Figs. 2(b) and 2(c) are fits to these forms.

Figure 4(b) demonstrates that H_{c3} exists up to fields greatly in excess of the 55 kG available in the QD SQUID magnetometer. Due to the large angular uncertainty associated with the mounting of the sample these data are not too useful in determining the value of H^0_{c3}, but as shown by the solid line, the above form, $H_{c3}=H^0_{c3}/\sin\phi$ with $H^0_{c3}=6.6$ kG, describes the data adequately. The most important feature of the data in Fig. 4(b) is that H_{c3} is still detectable up to 100 kG, and shows no indication of saturation.

The angular dependence of H_{c1} is easily understood in light of the Ho moments being primarily along the [110] axes. The applied magnetic-field-dependent energy difference between the zero-field antiferromagnetic structure ($\uparrow\downarrow\uparrow\downarrow\uparrow\downarrow$) and the first metamagnetic structure ($\uparrow\uparrow\downarrow\uparrow\uparrow\downarrow$) with 1/3 of the full Ho moment along the [110] axis (see Fig. 6) will vary as $H^*\mu_{sat}\cos(\theta)/3$. (It should be noted that moments along the [110] are shown as $\uparrow$ and moments along the [$\bar{1}10$] are shown as $\downarrow$.) If there is a critical energy difference, E_{CRIT}, that has to be exceeded to stabilize the first metamagnetic state, then the critical field will vary as $3*E_{CRIT}/\mu_{sat}*\cos(\theta)$. Simply stated, the moments being along the [110] axis easily explains a $1/\cos(\theta)$ angular dependence.

At first, the angular dependences of H_{c2} and H_{c3} are seemingly not so simply understood. Two obvious questions arise: (i) Why do H_{c2} and H_{c3} seem to depend on the angle ϕ from the [100] axis instead of the angle θ from the [110]

axis? and (ii) Why does H_{c3} diverge as $1/\sin(\phi)$? The answer to both of these questions lies in the nature of the magnetic order associated with the metamagnetic state that exists between H_{c2} and H_{c3}. If this metamagnetic state has an order that has a net distribution of moments ($\uparrow\uparrow\rightarrow\uparrow\uparrow\rightarrow$) along the [110] axes (see Fig. 6), where $\rightarrow$ represents the moment being along the [$\bar{1}10$] direction, then the angular dependences of H_{c2} and H_{c3} are trivially explained by the same argument used above for H_{c1}. The energy difference between the first and second metamagnetic states will be $H^*\mu_{sat}(2\cos\theta+\sin\theta-\cos\theta)/3=\sqrt{2}/3\ H^*\mu_{sat}\cos(45-\theta)=\sqrt{2}/3\ H^*\mu_{sat}\cos\phi$. This gives rise to $H_{c2}\propto1/\cos\phi$. In a similar manner the energy difference between the second metamagnetic state ($\uparrow\uparrow\rightarrow\uparrow\uparrow\rightarrow$) and the saturated paramagnetic state ($\uparrow\uparrow\uparrow\uparrow\uparrow\uparrow$) will be $H^*\mu_{sat}[\cos\theta-(2\cos\theta+\sin\theta)/3]=\sqrt{2}/3\ H^*\mu_{sat}\sin(45-\theta)=\sqrt{2}/3\ H^*\mu_{sat}\sin\phi$. This gives rise to $H_{c3}\propto1/\sin\phi$.

The net distribution of Ho moments then can have four possible configurations which are shown schematically in Fig. 6. For $H<H_{c1}$ the net distribution of moments is ($\uparrow\downarrow\uparrow\downarrow\uparrow\downarrow$). For $H_{c1}<H<H_{c2}$ the net distribution of moments is ($\uparrow\uparrow\downarrow\uparrow\uparrow\downarrow$). For $H_{c3}<H_{c3}$ the net distribution of moments is ($\uparrow\uparrow\rightarrow\uparrow\uparrow\rightarrow$), and for $H_{c3}<H$ the net distribution of moments is ($\uparrow\uparrow\uparrow\uparrow\uparrow\uparrow$). This series of net distributions of Ho moments along the [110] axes fully explains the angular dependence of the critical fields H_{c1}, H_{c2}, and H_{c3} as well as the simple angular dependences of M_{sat1} and M_{sat}. It should be emphasized that, at this point, we describe the arrangement of moments as net distributions of moments rather than structures. No assumption about the nature (wave vector) of the long-range ordered structure has been made.

Two data sets still need to be examined in light of this simple framework of net moments: M_{sat2} and ΔM_3. M_{sat2} would be expected to vary as $\mu_{sat}(2\cos\theta+\sin\theta)/3$. This angular dependence, shown as the solid line in Fig. 5(c), does not fit the data well. This may be due to a failure of our simple model of the net moments between H_{c2} and H_{c3}, but it is more likely that this is symptomatic of the fact that the saturated moment between these two fields is extremely hard to determine experimentally.

ΔM_3 is expected to vary as the difference between M_{sat} and M_{sat2}: $\Delta M_3=\mu_{sat}(\cos\theta-\sin\theta)/3=\sqrt{2}\mu_{sat}\sin(45-\theta)/3=\sqrt{2}\mu_{sat}\sin\phi/3$. In Fig. 5(d) this angular dependence, shown as a solid line, fits the data remarkably well. The agreement of this prediction with the data gives further support to the hypothesis that the experimental determination of H_{sat2} is flawed and that the choice of ($\uparrow\uparrow\rightarrow\uparrow\uparrow\rightarrow$) for the net moment distribution for $H_{c2}<H<H_{c3}$ is correct.

The net distribution of moments and the angular dependences of H_{ci} need to be examined theoretically and experimentally. In specific the values of H^0_{ci} as well as the fact that H_{c2} and H_{c3} merge, allowing for a transition from ($\uparrow\uparrow\downarrow\uparrow\uparrow\downarrow$) to ($\uparrow\uparrow\uparrow\uparrow\uparrow\uparrow$) for small θ, provide well defined parameters for theoretical analysis of the $HoNi_2B_2C$ system. The extreme anisotropy of the of the local Ho moment (only four positions) makes this a particularly simple magnetic system. Field-dependent neutron-diffraction and/or magnetic x-ray-diffraction measurements need to be performed on single crystals to determine the wave vectors of the ordering associated with the net distributions of moments described

above. Once this microscopic data is available, detailed theoretical analysis of this system should be fruitful.

CONCLUSIONS

Detailed measurements of $M(2\,\text{K}, H, T)$ for applied fields in the tetragonal a-b plane of $HoNi_2B_2C$ have revealed remarkably simple angular dependences of three metamagnetic states. The critical fields vary with the angle the applied field makes with the nearest $[110]$ axis, θ, and the nearest $[100]$ axis, ϕ, as $H_{ci}=4.1$ kG$/\cos\theta$, $H_{c2}=8.4/\cos\phi$, and $H_{c3}=6.6$ kG$/\sin\phi$. The locally saturated moments vary as $M_{\text{sat}}=9.85\mu_B\cos\theta$ for $H>H_{c3}$, and $M_{\text{sat1}}=3.25\mu_B\cos\theta$ for $H_{c1}<H<H_{c2}$. These angular dependences of the critical fields and saturated moments are consistent with a series of net distributions of Ho^{3+} moments as follows: $(\uparrow\downarrow\uparrow\downarrow\uparrow\downarrow)$ for $H<H_{c1}$, $(\uparrow\uparrow\downarrow\uparrow\uparrow\downarrow)$ for $H_{c1}<H<H_{c2}$, $(\uparrow\uparrow\rightarrow\uparrow\uparrow\rightarrow)$ for $H_{c2}<H<H_{c3}$, and $(\uparrow\uparrow\uparrow\uparrow\uparrow\uparrow)$ for $H>H_{c3}$, with the moments solely along $[110]$ axes. Field-dependent neutron diffraction or magnetic x-ray-scattering measurements will be needed to provide the microscopic data needed to test these simple hypothetical net distributions of moments.

*On leave from Centro Brasileiro de Pesquisas Fisicas, Rio de Janero, Brazil.

†Present address: Department of Chemistry, Cornell University, Ithaca, NY.

[1] R. J. Cava *et al.*, Nature (London) **376**, 252 (1994).

[2] M. Xu, P. C. Canfield, J. E. Ostenson, D. K. Finnemore, B. K. Cho, Z. R. Wang, and D. C. Johnston, Physica C **227**, 321 (1994).

[3] H. Eisaki *et al.*, Phys. Rev. B **50**, 647 (1994).

[4] B. K. Cho, M. Xu, P. C. Canfield, L. L. Miller, and D. C. Johnston, Phys. Rev. B **52**, 3676 (1995).

[5] R. Movshovich, M. F. Hundley, J. D. Thompson, P. C. Canfield, B. K. Cho, and A. V. Chubukov, Physica C **227**, 381 (1994).

[6] B. K. Cho, P. C. Canfield, L. L. Miller, D. C. Johnston, W. P. Beyermann, and A. Yatskar, Phys. Rev. B **52**, 3684 (1995).

[7] P. C. Canfield, B. K. Cho, D. C. Johnston, D. K. Finnemore, and M. F. Hundley, Physica C **230**, 397 (1994).

[8] K. D. D. Rathnayaka, D. G. Naugle, B. K. Cho, and P. C. Canfield, Phys. Rev. B **53**, 5688 (1996).

[9] B. K. Cho, P. C. Canfield, and D. C. Johnston, Phys. Rev. B **52**, R3844 (1995); P. Dervenagas, J. Zarestky, C. Stassis, A. I. Goldman, P. C. Canfield, and B. K. Cho, Physica B **212**, 1 (1995).

[10] A. Yatskar, N. K. Budraa, W. P. Beyermann, P. C. Canfield, and S. L. Bud'ko, Phys. Rev. B **54**, R3772 (1996).

[11] B. K. Cho, P. C. Canfield, and D. C. Johnston, Phys. Rev. B **53**, 8499 (1996).

[12] P. C. Canfield, B. K. Cho, and K. W. Dennis, Physica B **215**, 337 (1995).

[13] J. Zarestky, C. Stassis, A. I. Goldman, P. C. Canfield, P. Dervenagas, B. K. Cho, and D. C. Johnston, Phys. Rev. B **51**, 678 (1995).

[14] A. I. Goldman, C. Stassis, P. C. Canfield, J. Zarestky, P. Dervenagas, B. K. Cho, and D. C. Johnston, and B. Sternlieb, Phys. Rev. B **50**, 9668 (1994); C. Stassis, A. I. Goldman, P. Dervenagas, J. Zarestky, P. C. Canfield, B. K. Cho, D. C. Johnston, and B. Sternlieb, in *Neutron Scattering in Materials Science*, edited by D. A. Newmann, T. P. Russell, and B. J. Wuensch, MRS Symposia Proceedings No. 376 (Materials Research Society, Pittsburgh, 1995), p. 559.

[15] B. K. Cho, B. N. Harmon, D. C. Johnston, and P. C. Canfield, Phys. Rev. B **53**, 2217 (1996).

[16] P. Dervenagas, J. Zarestky, C. Stassis, A. I. Goldman, P. C. Canfield, and B. K. Cho, Phys. Rev. B **53**, 8506 (1996).

[17] P. C. Canfield, B. K. Cho, D. C. Johnston, M. F. Hundley, in *Neutron Scattering in Materials Science* (Ref. 14), p. 565.

[18] T. Siegrist *et al.*, Nature (London) **376**, 254 (1994).